Electronic Structure and TDDFT Optical Absorption Spectra of Silver Nanorods[†]

Hannah E. Johnson and Christine M. Aikens*

Department of Chemistry, Kansas State University, 213 CBC Building, Manhattan, Kansas 66506

Received: December 15, 2008; Revised Manuscript Received: January 28, 2009

Density functional theory calculations are employed to determine optimized geometries and excitation spectra for small pentagonal silver nanorods Ag_n, with $n = 13$, 19, 25, 31, 37, 43, 49, 55, 61, and 67 in various charge states. The asymptotically correct SAOP functional is utilized in the excitation calculations. Silver nanorods exhibit a sharp longitudinal excitation that results from a mixture of orbital transitions; the wavelength for this excitation depends linearly on the length of the nanorod. The broad transverse excitation arises from multiple excited states. A particle-in-a-box model is employed to explain the linear dependence of the longitudinal excitation wavelength on nanorod length.

Introduction

Noble metal nanoparticles (NPs) have many applications due to unique optical properties that arise when electrons are confined to the nanometer length scale. One of the notable characteristics of these nanoparticles is strong surface plasmon absorption that leads to a sharp peak in the visible region of the optical spectrum. As a consequence, gold and silver NPs can be employed in sensing techniques such as surface-enhanced Raman scattering (SERS).[1−5] In addition, gold nanorods are useful in cancer diagnostics and therapy due to their tunable absorption properties in the near-infrared region.[6,7] In general, the optical properties of NPs depend sensitively on their size and shape.[8,9]

Whether silver particles of various sizes display molecular or collective behavior is a question of interest to many researchers. The absorption spectra of small silver clusters Ag_n ($n = 2-21$) in rare gas matrixes depend on the number of atoms in the cluster for $n \leq 11$[10,11] but appear to exhibit collective behavior for $n \geq 13$.[10] Recent time-dependent density functional theory (TDDFT) studies of silver tetrahedra with 10−120 atoms suggest that in certain cases no disconnect exists between TDDFT computations for small systems and experimental measurements or continuum electrodynamics calculations for larger systems.[12] Time-dependent local density approximation calculations using a jellium model have been employed for silver and gold systems and generally agree with Mie theory on the size dependence of the location of the plasmon resonance.[13−15]

Optical absorption spectra for nanorods display two bands (corresponding to excitation in the longitudinal and transverse directions), and it has been found empirically that the wavelength of the strong longitudinal plasmon resonance band depends linearly on aspect ratio (length to diameter).[16,17] Significant synthetic control over aspect ratio has been achieved; for instance, silver nanorods and nanowires can be prepared with aspect ratios of 2.5−10 and 50−350, respectively, using a seed-mediated synthesis.[18]

Band gaps of semiconductor nanowires depend on the diameter d of the wire.[19,20] Empirically, the band gaps of indium phosphide[19] and cadmium selenide[20] are determined to vary as $d^{-1.45}$ and $d^{-1.36}$, respectively. A particle-in-a-cylinder model has been employed to explain this dependence, and shows that the energy depends on $(\phi_{n,l}^2/d^2)$, where $\phi_{n,l}$ is the nth root of the lth-order cylindrical Bessel function, and on the band gap of the bulk material.[21] This analysis did not discuss length dependence, because the semiconductor nanowires are several micrometers in length.[21] However, a similar model capable of treating finite-length noble metal nanorods is of interest due to the sensitive dependence of the longitudinal excitation on aspect ratio. Previous particle-in-a-cylinder models have been used to examine plasmon widths and oscillator strengths.[22]

In this work, the optical absorption spectra and origin of the linearity in the longitudinal peak energy with respect to system size are examined for a series of silver nanorods with 13−67 atoms. Pentagonal nanorods are considered because noble metal nanorods often have decahedral symmetry,[23,24] and 5-fold axes are also ubiquitous in other nanomaterials such as monolayer-protected gold nanoparticles (e.g., $Au_{102}(SR)_{44}$[25] and $Au_{25}(SR)_{18}$[26−28] with decahedral and icosahedral cores, respectively) and noble metal nanodecahedra.[29,30]

Computational Details

The calculations described in this work are performed with the Amsterdam Density Functional (ADF) 2007.01 program.[31] The molecular structures of all neutral and charged clusters are optimized with C_{5v} symmetry using the gradient-corrected Becke−Perdew (BP86) exchange-correlation functional.[32,33] The basis set employed in the optimizations is a double-ζ (DZ) Slater type basis set with a $[1s^2-4p^6]$ frozen core for Ag (denoted DZ.4p). Scalar relativistic effects are included by utilizing the zeroth-order regular approximation (ZORA).[34] Time-dependent density functional theory (TDDFT) is employed to determine energetics and compositions of excited states using the asymptotically correct statistical average of orbital potentials (SAOP)[35,36] and LB94[37] model potentials as well as the BP86 functional. The basis set utilized in the SAOP calculations is an all-electron DZ basis set, and orbitals are numbered according to the SAOP/DZ ordering. The ADF-GUI program is used for orbital visualization. Depending on the size of the nanorod, the first 100−1500 dipole-allowed transitions are evaluated for the optical absorption spectrum. Increasing the number of excited states in the calculation leads to negligible changes in the energies and oscillator strengths for low energy transitions relative to calculations involving fewer states; these errors are typically in the third decimal place or below. Because of the

[†] Part of the "George C. Schatz Festschrift".

10.1021/jp811075u CCC: $40.75
Published on Web 03/18/2009

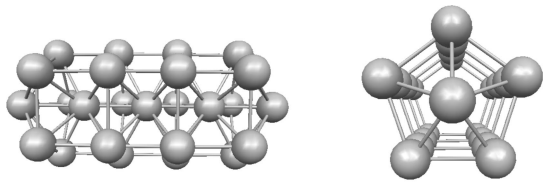

Figure 1. Pentagonal silver nanorod with 25 atoms.

large number of excited states below 5 eV in these metal clusters, absolute errors in predicted energies for the high energy states in this range are expected to be smaller than the absolute errors due to functional and basis set approximations. The smoothed spectra shown in the figures are convoluted with a Lorentzian with a full width at half-maximum (fwhm) of 0.2 eV.

Several computational parameters were adjusted to improve the numerical accuracy of the calculations. The SCF convergence was tightened to 10^{-8}. A gradient convergence criterion of 10^{-3} or tighter and an energy convergence criterion of 10^{-4} or tighter were used in order to obtain well-converged geometries. The error tolerance in the square of the excitation energies was set to 10^{-8}, and the orthonormality of the Davidson trial vectors was set to 10^{-10}. The numerical integration accuracy of integrals for the Fock matrix elements and energy terms was improved to 10^{-6}. These technical parameter adjustments have been found to yield changes in the second decimal place of the predicted excitation energies.

Results and Discussion

Geometric and Electronic Structure of a 25-Atom Silver Nanorod. The nanorods examined in this work exhibit many similarities, so this paper will first describe in detail a representative nanorod with 25 atoms and then discuss the size dependence of the optical absorption of these systems.

A decahedral arrangement of 25 atoms can be constructed by considering a central core of five atoms surrounded by four pentagons (Figure 1). At the BP86/DZ.4p level of theory, the nearest neighbor distances in the core range from 2.85 to 2.89 Å and distances between parallel pentagons vary from 2.77 to 2.83 Å, while nearest neighbor distances within a pentagon range from 2.91 to 2.97 Å. The neutral Ag_{25} nanorod has a single unpaired electron in the highest occupied molecular orbital (HOMO), which is a singly degenerate a_1 orbital. The nanorods with 19 and 43 atoms have a similar arrangement; however, the neutral nanorods with 31, 37, 49, 55, 61, and 67 atoms would have a single unpaired electron in a doubly degenerate orbital. To avoid Jahn−Teller distortions, charge states of the nanorods corresponding to completely filled orbitals are of interest. This procedure was previously shown to yield sharp absorption spectra for silver tetrahedra.[12] For Ag_{25}, charge states of −1, +1, and +5 are reasonable based solely on electronic structure considerations.

The optimized geometry of Ag_{25}^{+1} is similar to that of neutral Ag_{25}. Nearest neighbor distances in the core are predicted to be 2.82−2.84 Å, while distances between pentagons range from 2.76 to 2.84 Å and nearest neighbor distances within pentagons vary from 2.93 to 2.98 Å. For Ag_{25}^{-1}, these ranges are 2.84−2.92, 2.77−2.82, and 2.91−2.97 Å, respectively, in close agreement to Ag_{25}^{0} and Ag_{25}^{+1}. Ag_{25}^{+5} is relatively elongated along the long axis of the nanorod and slightly contracted along the short axis; the corresponding distances for this system are 2.88−3.17, 3.02−3.04, and 2.86−2.93 Å, respectively.

The HOMO−LUMO gap of Ag_{25}^{+1} is 0.30 eV at the SAOP/DZ level of theory. The gap for Ag_{25}^{-1} is 0.07 eV, and the gap for Ag_{25}^{+5} is 0.80 eV. For all nanorods considered in this work, the HOMO−LUMO gap is finite. The longest nanorod discussed here is Ag_{67}^{+1}, which possesses a HOMO−LUMO gap of 0.20 eV. It is important to emphasize that, even though silver is metallic in its bulk phase, confined systems such as nanorods typically have band gaps.

Orbitals and Transitions Contributing to Optical Absorption Spectra. The SAOP/DZ optical absorption spectra for Ag_{25}^{+1}, Ag_{25}^{-1}, and Ag_{25}^{+5} are presented in Figure 2. Each absorption spectrum exhibits a relatively sharp peak between 3.3 and 3.4 eV in addition to a broader peak between 4.1 and 4.6 eV. Similar absorption spectra for the other nanorods are shown in Supporting Information Figure S1. Regardless of the nanorod under consideration, the lower energy peak arises from one or more excited states with A_1 symmetry, whereas the higher energy peak has E_1 symmetry and typically evolves from multiple excited states. These two peaks correspond to transitions from the *z*- (long axis) and (*x*,*y*)- (short axis) components of the electric dipole operator, respectively, and are therefore direct analogs of the longitudinal and transverse polarization peaks observed experimentally.

Because all of the nanorods examined in this work can achieve a +1 charge state, this charge state of Ag_{25} is discussed in detail in this section. The primary orbital transitions responsible for the strong peaks in the absorption spectrum of Ag_{25}^{+1} are shown in Table 1, and the orbital energy diagram and Kohn−Sham orbitals are displayed in Figure 3. Because of the approximate cylindrical symmetry of the nanorods, uppercase Greek letters Σ, Π, Δ, Φ, etc., may be used to describe the angular momentum of the orbitals. The Kohn−Sham orbitals for Ag_{25}^{+1} are comprised of a set of Σ orbitals (Figure 3, blue solid) with nodal planes perpendicular to the long axis of the nanorod, a set of degenerate pairs of Π orbitals (Figure 3, green dot-dashed) with a single nodal plane containing the long axis in addition to nodes perpendicular to the axis, a set of degenerate pairs of Δ orbitals (Figure 3, black dotted) with two nodal planes that contain the long axis, and a second set of Σ orbitals (denoted 2Σ in Figure 3, purple dashed) that possess a radial node in addition to nodes perpendicular to the long axis. These orbitals have a_1, e_1, e_2, and a_1 symmetry, respectively, in the C_{5v} point group. In addition, Φ orbitals (with three nodal planes that contain the long axis) (Figure 4) and a second set of Π orbitals are also present at higher energies. The subscript on each Greek letter refers to the number of longitudinal nodes in the orbital plus 1. Similar Σ, Π, Δ, etc., orbitals are also observed for longer nanorods (Supporting Information Figure S2).

The strongest absorption peak for Ag_{25}^{+1} lies at 3.40 eV and arises from mixed $e_1 \rightarrow e_1$ ($\Pi \rightarrow \Pi$) and $a_1 \rightarrow a_1$ ($\Sigma \rightarrow \Sigma$) transitions (Table 1). The corresponding strong A_1 peak for nanorods of other lengths also arises from mixed $e_1 \rightarrow e_1$ and $a_1 \rightarrow a_1$ transitions. In fact, all of the strong peaks arise from mixed transitions. For the primary transitions of each strong peak, the *z*-components of the transition dipole moment have the same sign; this agrees well with the classical picture of formation of a dipole in the *z*-direction upon excitation with radiation polarized along this axis. Each mixed transition also yields one or more states at lower energy that correspond to the same primary orbital transitions with opposing contributions to the transition dipole moment; for Ag_{25}^{+1}, there are two weak low energy states of interest because a linear combination of

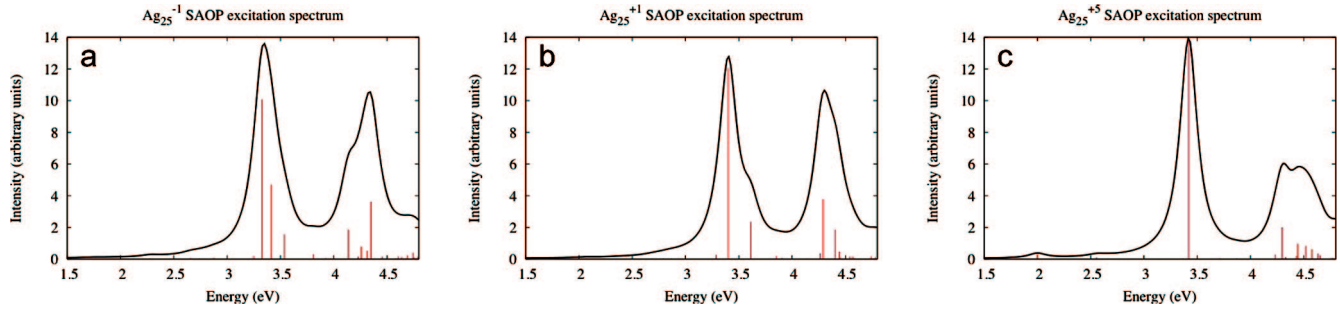

Figure 2. TDDFT absorption spectra for (a) Ag_{25}^{-1}, (b) Ag_{25}^{+1}, and (c) Ag_{25}^{+5}.

TABLE 1: Strong Optical Absorption Peaks in the Spectrum of Ag_{25}^{+1}; the Symmetries, Oscillator Strengths, and Degeneracies (g) of These States; and the Primary Transitions Responsible for These Peaks

peak energy (eV)	excited-state symmetry	oscillator strength (g)	transition from occupied orbital	transition to unoccupied orbital	weight
3.40	A_1	3.787	$120e_1$ (HOMO−1)	$121e_1$ (LUMO+4)	0.4048
			$113a_1$ (HOMO−2)	$114a_1$ (LUMO)	0.1821
			$113a_1$ (HOMO−2)	$115a_1$ (LUMO+2)	0.1405
3.61	A_1	0.7401	$113a_1$ (HOMO−2)	$118a_1$ (LUMO+7)	0.3792
			$103e_2$ (HOMO)	$108e_2$ (LUMO+14)	0.4585
4.29	E_1	1.188 (2)	$120e_1$ (HOMO−1)	$120a_1$ (LUMO+15)	0.2459
			$103e_2$ (HOMO)	$106e_2$ (LUMO+10)	0.1132
4.40	E_1	0.5822 (2)	$120e_1$ (HOMO−1)	$120a_1$ (LUMO+15)	0.6175
			$103e_2$ (HOMO)	$109e_2$ (LUMO+16)	0.0513

three orbital transitions must yield three states. These states and the z-components of their transition dipole moments are shown in Table 2.

For several other nanorods, $e_2 \rightarrow e_2$ ($\Delta \rightarrow \Delta$) transitions also contribute to the longitudinal peak; e.g., for Ag_{55}^{+1}, $e_2 \rightarrow e_2$ transitions mix with the $e_1 \rightarrow e_1$ and $a_1 \rightarrow a_1$ transitions. The second A_1 peak for Ag_{25}^{+1} also involves mixed $a_1 \rightarrow a_1$ and $e_2 \rightarrow e_2$ transitions. Because this peak involves a transition out of the HOMO ($103e_2$), this peak does not appear in the corresponding Ag_{25}^{+5} spectrum, since this orbital is not occupied in the +5 charge state. Although the overall features are similar for nanorods with different charge states, the differences in orbital occupations greatly affect the possible transitions and hence excited-state composition. This can lead to heterogeneity in experimental systems, which are composed of a distribution of lengths and possibly several charge states.

The transverse E_1 peak for Ag_{25}^{+1} arises from mixed $e_1 \rightarrow a_1$ ($\Pi \rightarrow \Sigma$) and $e_2 \rightarrow e_2$ ($\Delta \rightarrow \Phi$) transitions. Overall, $e_1 \rightarrow a_1$ transitions are more common than $a_1 \rightarrow e_1$ ($\Sigma \rightarrow \Pi$) transitions, although both contribute to the E_1 peak for nanorods of other sizes. In addition, the E_1 peak sometimes involves $e_1 \rightarrow e_2$ transitions. Overall, the transverse peak arises from many different excited states that involve several orbital transitions, which may explain why this peak is broad and does not exhibit clear size-dependent behavior, as discussed in the next section.

Size Dependence of Optical Absorption Spectra. The longest system examined in this work is a pentagonal nanorod with 67 atoms, which possesses 12 core atoms and 11 parallel pentagons. The diameter of this rod is 0.8 nm, and the length is 3.4 nm (calculated by adding the bulk nearest neighbor Ag−Ag distance of 0.289 nm as an estimate of twice the atomic radius to the distances determined from the nuclear coordinates), which leads to an approximate aspect ratio of 4.3. Ag_{13}^{+1}, the shortest system examined in this work, has a length of 0.9 nm and an approximate aspect ratio of 1.1.

The SAOP/DZ excitation spectra for a collection of nanorods in the +1 charge state are shown in Figure 5. (Individual spectra for each size of nanorod are available in Supporting Information Figure S1.) Ag_{13}^{+1} does not exhibit an E_1 peak and is therefore not included in Figure 5. As noted previously for silver tetrahedra,[12] TDDFT computations for small systems and experimental measurements or continuum electrodynamics calculations for larger systems agree on the important features of the systems. In accord with previously observed trends for nanorods,[17,18] the energy of the longitudinal A_1 peak monotonically shifts to the red as the length increases. For the systems considered here, the energy of this peak ranges from 2.09 to 3.73 eV. A linear relationship is evident between the wavelength of the longitudinal peak and the number of atoms in the core (Figure 6). The intensity of the A_1 peak also increases linearly with the number of electrons in the nanorod. The energy of the transverse E_1 peak changes slightly with nanorod length, but the shift is not monotonic and the energy range is smaller (4.25−4.45 eV). In silver nanorod solutions, the transverse peak falls at 400 nm (3.1 eV) for 10−15 nm diameter rods,[18] and the smaller diameter (0.8 nm) of the nanorods examined in this work likely accounts for the relative blue-shift observed here.

The predicted energy of the A_1 and E_1 peaks depends strongly on the functional employed in the calculations. For example, the longitudinal peak of Ag_{19}^{+1} is predicted to lie at 3.57, 3.35, and 4.05 eV at the SAOP/DZ, BP86/DZ.4p, and LB94/DZ.4p levels of theory. The value predicted with the BP86 functional differs by 0.2 eV from that determined with the SAOP functional, whereas LB94 overestimates the excitation by 0.5 eV relative to SAOP values. A similar trend was previously observed for a Ag_{20} tetrahedral cluster.[12] The relative difference decreases as the nanorod length increases; for Ag_{67}^{+1}, the predicted A_1 peak energies are 2.09, 2.08, and 2.21 eV at the SAOP/DZ, BP86/DZ.4p, and LB94/DZ.4p levels of theory. However, the ratio of the wavelength to the number of core atoms varies markedly with the functional employed. The best-fit lines for BP86 and SAOP (Figure 6) appear to cross at Ag_{67}^{+1}, so the close agreement determined for this system may be accidental. The slopes of the LB94 and SAOP best-fit lines are nearly identical, which suggests that LB94 may describe the nanorod size dependence as well as SAOP and could be a less computationally expensive alternative after accounting for the difference in intercepts.

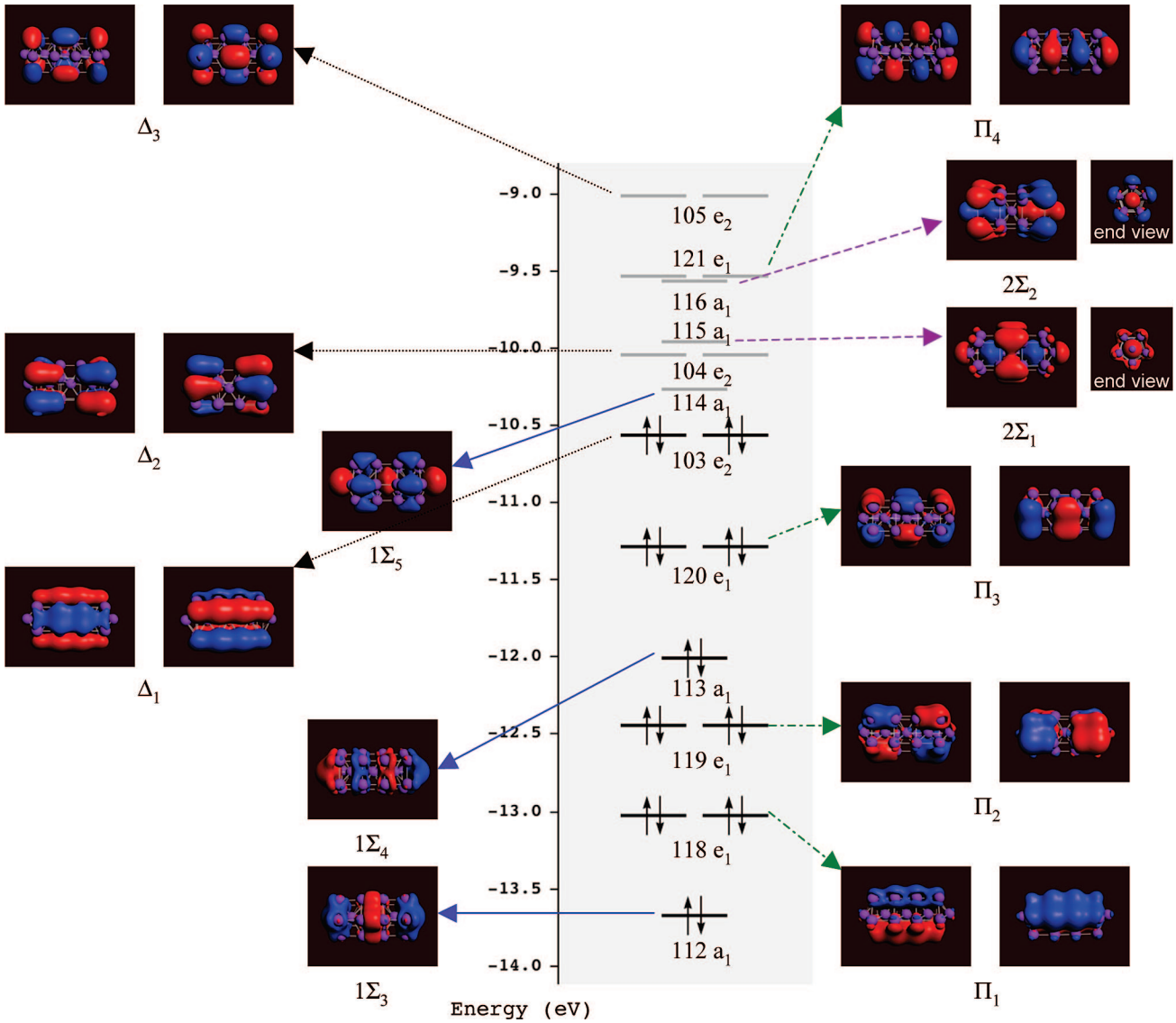

Figure 3. SAOP/DZ Kohn−Sham orbitals and orbital energy diagram for Ag_{25}^{+1}. The orbitals are plotted with a contour value of 0.15.

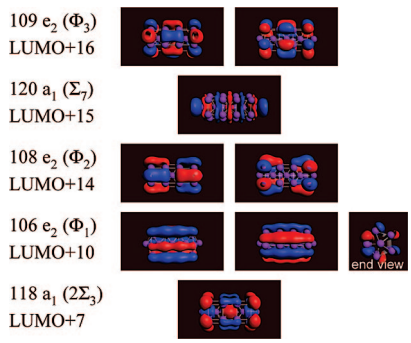

Figure 4. Selected unoccupied SAOP/DZ Kohn−Sham orbitals for Ag_{25}^{+1}. The orbitals are plotted with a contour value of 0.15.

TABLE 2: Optical Absorption Peaks in the Spectrum of Ag_{25}^{+1} with the Same Orbital Transitions

peak energy (eV)	oscillator strength	transition from occupied orbital	transition to unoccupied orbital	weight	*z*-component of transition dipole moment
1.85	0.0003	$113a_1$	$114a_1$	0.7306	−5.489
		$120e_1$	$121e_1$	0.2584	4.958
2.07	0.012	$113a_1$	$115a_1$	0.8171	4.316
		$120e_1$	$121e_1$	0.1485	−3.556
3.40	3.787	$120e_1$	$121e_1$	0.4048	4.580
		$113a_1$	$114a_1$	0.1821	2.023
		$113a_1$	$115a_1$	0.1405	1.397

Comparison with Particle-in-a-Box Analysis. A nanorod may be viewed as a system of electrons constrained by a cylindrical potential arising from the nuclei. The potential may be considered to have the form

$$V(r,\phi,z) = 0\begin{cases} 0 \le r < R \\ 0 \le \phi \le 2\pi \\ 0 < z < l \end{cases} = \infty\{\text{otherwise} \qquad (1)$$

where R and l are the radius and length of the cylinder, respectively. The time-independent Schrödinger equation for an electron in this potential is $(-\hbar^2/2m)\nabla^2\psi = E\psi$, where the Laplacian (in cylindrical coordinates) is written

$$\nabla^2 = \frac{1}{r}\frac{\partial}{\partial r} + \frac{\partial^2}{\partial r^2} + \frac{1}{r^2}\frac{\partial^2}{\partial \phi^2} + \frac{\partial^2}{\partial z^2} \qquad (2)$$

By applying the method of separation of variables and assuming the solution is in the form $\psi(r,\phi,z) = F(r)\,G(\phi)\,H(z)$, three differential equations involving the axial (z), azimuthal (ϕ), and

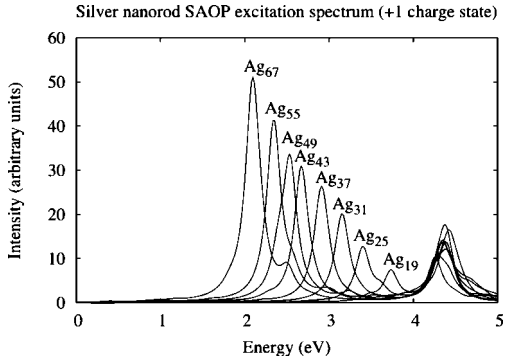

Figure 5. SAOP/DZ absorption spectrum of silver nanorods in the +1 charge state.

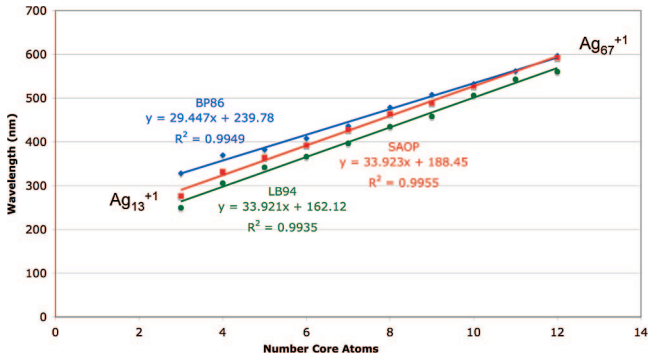

Figure 6. Wavelength of the longitudinal A_1 peak versus the number of atoms in the core. Data and best-fit lines are shown for the BP86 (blue diamonds), SAOP (red squares), and LB94 (green circles) functionals.

radial (r) variables arise. The axial differential equation is equivalent to the one-dimensional particle-in-a-box equation. The full particle-in-a-cylinder solutions involve the roots of the cylindrical Bessel functions (see refs 21 and 22). However, a simple approximation can be employed to explain the linear relationship between nanorod length and excitation wavelength.

The energy of an electron in the cylindrical potential may be written as the sum $E = E_{r\phi} + E_z$, where $E_{r\phi}$ is the energy obtained by solving the azimuthal and radial differential equations and E_z is the energy obtained from the solution of the particle-in-a-box problem. Due to group theoretical considerations, the longitudinal transitions in a nanorod must involve $\Sigma \rightarrow \Sigma$, $\Pi \rightarrow \Pi$, or $\Delta \rightarrow \Delta$ transitions. Because these transitions do not involve changes in the azimuthal and radial quantum numbers, $E_{r\phi}$ is constant. Thus, energy differences can be written as a difference of two particle-in-a-box energies

$$E_n = \frac{n^2\hbar^2}{8ml^2} \qquad n = 1, 2, 3, \ldots \tag{3}$$

where n is the quantum number in the axial direction, m is the mass of the electron, and $\hbar$ is Planck's constant. For each nanorod, assume that the length l is proportional to the number of core atoms N

$$l = bN \tag{4}$$

where b is a proportionality constant. For the Σ transitions, the highest occupied level is Σ_{N-1}. For example, the highest occupied $1\Sigma_4$ orbital in Ag_{25}^{+1} has four orbital lobes, which is one less than the number of core atoms in the structure. A transition to unoccupied level Σ_N would have the energy

$$E_N - E_{N-1} = \frac{\hbar^2}{8ml^2}(N^2 - (N-1)^2) = \frac{\hbar^2}{8mb^2}\left(\frac{2}{N} - \frac{1}{N^2}\right) \tag{5}$$

where eq 4 was employed. The wavelength of the transition is thus

$$\lambda = \frac{c8mb^2}{\hbar}\left(\frac{1}{2}N + \frac{1}{4} + \frac{1}{8N-4}\right) \tag{6}$$

Equation 6 is essentially linear in N. The third term in parentheses in eq 6 expresses the nonlinearity, which decreases as the number of core atoms N increases. Comparable expressions can be written for Π and Δ transitions, and the wavelength can similarly be shown to effectively depend linearly on N.

Conclusion

The nodal structure of nanorod orbitals follows a particle-in-a-cylinder model. The orbitals have approximate cylindrical symmetry, and consist of sets of Σ, degenerate Π, degenerate Δ, and degenerate Φ orbitals with axial and radial nodes. The longitudinal A_1 excitation consists of a linear combination of $\Sigma \rightarrow \Sigma$ and $\Pi \rightarrow \Pi$ transitions (and possibly $\Delta \rightarrow \Delta$ transitions), where the z-components of the transition matrix elements have the same sign. The transverse E_1 excitation may be formed from $\Pi \rightarrow \Sigma$, $\Delta \rightarrow \Phi$, $\Sigma \rightarrow \Pi$, and $\Pi \rightarrow \Delta$ transitions. In addition, it is formed from multiple excited states and is in general much broader than the longitudinal peak. The transverse excitation has no clear size dependence for the systems examined here, whereas the wavelength and intensity of the longitudinal excitation depend linearly on the size of the nanorod. The relationship of the wavelength to nanorod length may be rationalized by a particle-in-a-box model.

Acknowledgment. The authors would like to thank Prof. William Buhro for sending a preprint of ref 21. C.M.A. would like to thank Kansas State University for start-up and seed funding that supported this research.

Supporting Information Available: Optical absorption spectra of all nanorods discussed in this work and Kohn−Sham orbitals and an orbital energy diagram for Ag_{67}^{+1}. This material is available free of charge via the Internet at http://pubs.acs.org.

References and Notes

(1) Jeanmaire, D. L.; Van Duyne, R. P. *J. Electroanal. Chem.* **1977**, *84*, 1.
(2) Haes, A. J.; Haynes, C. L.; McFarland, A. D.; Schatz, G. C.; Van Duyne, R. P.; Zou, S. *MRS Bull.* **2005**, *30*, 368.
(3) Kneipp, K.; Wang, Y.; Kneipp, H.; Perelman, L. T.; Itzkan, I.; Dasari, R. R.; Feld, M. S. *Phys. Rev. Lett.* **1997**, *78*, 1667.
(4) Michaels, A. M.; Nirmal, M.; Brus, L. E. *J. Am. Chem. Soc.* **1999**, *121*, 9932.
(5) Stuart, D. A.; Yuen, J. M.; Shah, N.; Lyandres, O.; Yonzon, C. R.; Glucksberg, M. R.; Walsh, J. T.; Van Duyne, R. P. *Anal. Chem.* **2006**, *78*, 7211.
(6) El-Sayed, I. H.; Huang, X.; El-Sayed, M. A. *Nano Lett.* **2005**, *5*, 829.
(7) Huang, X.; El-Sayed, I. H.; Qian, W.; El-Sayed, M. A. *J. Am. Chem. Soc.* **2006**, *128*, 2115.
(8) Kreibig, U.; Vollmer, M. Optical Properties of Metal Clusters; Springer: Berlin, 1995.

(9) Kelly, K. L.; Coronado, E.; Zhao, L. L.; Schatz, G. C. *J. Phys. Chem. B* **2003**, *107*, 668.
(10) Fedrigo, S.; Harbich, W.; Buttet, J. *Phys. Rev. B* **1993**, *47*, 10706.
(11) Conus, F.; Rodrigues, V.; Lecoultre, S.; Rydlo, A.; Félix, C. *J. Chem. Phys.* **2006**, *125*, 024511.
(12) Aikens, C. M.; Li, S.; Schatz, G. C. *J. Phys. Chem. C* **2008**, *112*, 11272.
(13) Prodan, E.; Nordlander, P.; Halas, N. J. *Nano Lett.* **2003**, *3*, 1411.
(14) Lermé, J.; Palpant, B.; Prével, B.; Pellarin, M.; Treilleux, M.; Vialle, J. L.; Perez, A.; Broyer, M. *Phys. Rev. Lett.* **1998**, *80*, 5105.
(15) Liebsch, A. *Phys. Rev. B* **1993**, *48*, 11317.
(16) Yu, Y.-Y.; Chang, S.-S.; Lee, C.-L.; Wang, C. R. C. *J. Phys. Chem. B* **1997**, *101*, 6661.
(17) Link, S.; Mohamed, M. B.; El-Sayed, M. A. *J. Phys. Chem. B* **1999**, *103*, 3073.
(18) Jana, N. R.; Gearheart, L.; Murphy, C. J. *Chem. Commun.* **2001**, 617.
(19) Yu, H.; Li, J.; Loomis, R. A.; Wang, L.-W.; Buhro, W. E. *Nat. Mater.* **2003**, *2*, 517.
(20) Yu, H.; Li, J.; Loomis, R. A.; Gibbons, P. C.; Wang, L.-W.; Buhro, W. E. *J. Am. Chem. Soc.* **2003**, *125*, 16168.
(21) Sun, J.; Buhro, W. E.; Wang, L.-W.; Schrier, J. *Nano Lett.* **2008**, *8*, 2913.
(22) Kraus, W. A.; Schatz, G. C. *J. Chem. Phys.* **1983**, *79*, 6130.
(23) Canizal, G.; Ascencio, J. A.; Gardea-Torresdey, J.; Yacamán, M. J. *J. Nanopart. Res.* **2001**, *3*, 475.
(24) Johnson, C. J.; Dujardin, E.; Davis, S. A.; Murphy, C. J.; Mann, S. *J. Mater. Chem.* **2002**, *12*, 1765.
(25) Jadzinsky, P. D.; Calero, G.; Ackerson, C. J.; Bushnell, D. A.; Kornberg, R. D. *Science* **2007**, *318*, 430.
(26) Heaven, M. W.; Dass, A.; White, P. S.; Holt, K. M.; Murray, R. W. *J. Am. Chem. Soc.* **2008**, *130*, 3754.
(27) Zhu, M.; Aikens, C. M.; Hollander, F. J.; Schatz, G. C.; Jin, R. *J. Am. Chem. Soc.* **2008**, *130*, 5883.
(28) Zhu, M.; Eckenhoff, W. T.; Pintauer, T.; Jin, R. *J. Phys. Chem. C* **2008**, *112*, 14221.
(29) Sánchez-Iglesias, A.; Pastoriza-Santos, I.; Pérez-Juste, J.; Rodríguez-González, B.; García de Abajo, F. J.; Liz-Marzán, L. M. *Adv. Mater.* **2006**, *18*, 2529.
(30) Seo, D.; Yoo, C. I.; Chung, I. S.; Park, S. M.; Ryu, S.; Song, H. *J. Phys. Chem. C* **2008**, *112*, 2469.
(31) te Velde, G.; Bickelhaupt, F. M.; Baerends, E. J.; Fonseca Guerra, C.; van Gisbergen, S. J. A.; Snijders, J. G.; Ziegler, T. *J. Comput. Chem.* **2001**, *22*, 931.
(32) Becke, A. D. *Phys. Rev. A* **1988**, *38*, 3098.
(33) Perdew, J. P. *Phys. Rev. B* **1986**, *33*, 8822.
(34) van Lenthe, E.; Baerends, E. J.; Snijders, J. G. *J. Chem. Phys.* **1993**, *99*, 4597.
(35) Gritsenko, O. V.; Schipper, P. R. T.; Baerends, E. J. *Chem. Phys. Lett.* **1999**, *302*, 199.
(36) Schipper, P. R. T.; Gritsenko, O. V.; van Gisbergen, S. J. A.; Baerends, E. J. *J. Chem. Phys.* **2000**, *112*, 1344.
(37) van Leeuwen, R.; Baerends, E. J. *Phys. Rev. A* **1994**, *49*, 2421.

JP811075U